The helminth parasite Fasciola hepatica modulates barrier integrity of human intestinal organoid-derived monolayers

Judit Serrat
Laboratory of Helminth Parasites of Zoonotic Importance (ATENEA), Institute of Natural Resources and Agrobiology of Salamanca (IRNASA-CSIC), Salamanca, Spain

Mar Siles-Lucas
Laboratory of Helminth Parasites of Zoonotic Importance (ATENEA), Institute of Natural Resources and Agrobiology of Salamanca (IRNASA-CSIC), Salamanca, Spain

Anton Aebischer
Department of Infectious Diseases, Unit for Mycotic and Parasitic Agents and Mycobacteria, Robert Koch Institute, Berlin, Germany

Christian Klotz
Department of Infectious Diseases, Unit for Mycotic and Parasitic Agents and Mycobacteria, Robert Koch Institute, Berlin, Germany

Javier González-Miguel
javier.gonzalez@irnasa.csic.es

Laboratory of Helminth Parasites of Zoonotic Importance (ATENEA), Institute of Natural Resources and Agrobiology of Salamanca (IRNASA-CSIC), Salamanca, Spain https://orcid.org/0000-0003-4279-4761

Article

Keywords:

Posted Date: January 16th, 2026

DOI: https://doi.org/10.21203/rs.3.rs-8602005/v1

Additional Declarations: There is **NO** Competing Interest.

Abstract

Migration of the helminth parasite *Fasciola hepatica* across the intestine is a critical determinant of infection success, yet the molecular mechanisms governing this process remain poorly understood. Here, we apply human organoid-derived monolayers (ODMs) to investigate early interactions between *F. hepatica* newly excysted juveniles (FhNEJ) and the intestinal epithelium. ODMs were stimulated with live FhNEJ, and barrier function was assessed using measurements of transepithelial electrical resistance, fluorescein flux assays, and immunofluorescent detection of tight junction proteins. Parasite-induced changes in host protein expression were further examined by proteomics. Results showed that FhNEJ actively engaged with the ODM epithelium and induced a time- and dose-dependent loss of barrier integrity, accompanied by reduced expression and apical localisation of zonula occludens-1, a key tight junction component. Proteomic profiling of ODMs identified additional differentially regulated proteins involved in cell adhesion, immunity, and intercellular junction organisation. Together, these results provide novel insights into how FhNEJ compromise intestinal barrier permeability and establish ODMs as a robust and physiologically relevant platform for dissecting the molecular events that underlie the intestinal phase of *F. hepatica* infection.

Introduction

The helminth trematode *Fasciola hepatica*, also known as the liver fluke, is the primary etiologic agent of fasciolosis, the most widely distributed food-borne trematodiasis worldwide, accounting for millions of infections in both animals and humans[1–3]. Definitive hosts typically become infected through ingestion of aquatic plants or water contaminated with metacercariae, which release newly excysted juveniles (FhNEJ) upon arrival to the duodenum. Around three to 72 hours after metacercariae excystment, FhNEJ cross the intestinal wall and migrate through the peritoneum until the parasites gain access to the liver and subsequently the major hepatic bile ducts, where adult flukes mature and produce eggs that are shed with faeces[4,5]. Since hyper-endemic areas of human fasciolosis are concentrated in tropical regions where people often live under substandard socio-economic conditions, human fasciolosis is classified by the World Health Organization as a neglected tropical disease of growing public health concern[3,6]. Moreover, by infecting millions of ruminants worldwide, *F. hepatica* poses a significant threat to animal welfare and global food security[2]. Despite its importance, the molecular mechanisms by which *F. hepatica* invades its host, particularly those involved in the early migration of juvenile parasites through the intestine, remain poorly understood, constraining the development of novel control measures[7].

Over the past recent years, there has been a steady increase in the number of cases of fasciolosis in which the parasite was resistant to the drug of choice, triclabendazole, raising awareness on the need to find alternative treatment and control strategies[8–10]. Given that most tissue damage caused by *F. hepatica* infection results from post-intestinal migration of juvenile flukes across the peritoneum and the hepatic parenchyma before their establishment within the bile ducts[4], new approaches to mitigate the

pathology associated with fasciolosis should focus on blocking the trans-intestinal migration of newly-excysted parasites. However, a thorough understanding about the mechanisms that FhNEJ employ to cross the intestinal wall is still lacking, mainly due to limitations of current *in vitro* models to resemble the *in vivo* situation [11,12]. For example, primary epithelial cells derived from the mouse small intestine have been co-cultured with FhNEJ to replicate the parasite–gut interface, providing important insights into the molecular responses that are triggered in the intestinal epithelium upon infection [13]. However, the culture of intestinal primary cells from mice fails to reproduce the architecture, polarisation, and the multicellular complexity of the tissue, limiting the physiological relevance of the results in the mammalian context [11]. Likewise, *in vivo* and *ex vivo* animal models employing whole-tissue sections are also available to study the initial stages of *F. hepatica* infection [14,15], but they do not entirely reflect the human situation and do not comply with current European 3R guidelines to reduce the use of animals for research purposes [16]. Furthermore, analysis at the whole-tissue level dilutes the highly localised epithelial responses occurring at sites of direct parasite contact, hindering precise analysis of parasite-induced changes in intestinal barrier integrity and epithelial function.

Three-dimensional (3D) organoids and related *in vitro* systems have emerged as promising alternatives for the study of host–parasite interactions during infection with clinically-relevant helminths[17–19]. For instance, co-culture of FhNEJ with spheroids derived from a hepatocyte cell line that recreate the microenvironment of the liver parenchyma has been shown to support parasite survival and growth [20], offering the opportunity to interrogate the molecular pathways that drive parasite development within the mammalian host. In the context of the intestine, organoids have also been developed from gastrointestinal tissues of different species to investigate host–helminth interactions, providing physiologically relevant models that reproduce the cellular composition of the epithelium and enabling experimental infection with parasitic nematodes of clinical importance [17–19]. These systems are based on the isolation of intestinal stem cells from samples obtained from healthy donors and their subsequent expansion and differentiation into 3D structures that provide a more physiologically-relevant system to model the intestinal epithelium *in vitro*. However, the applicability of 3D organoids for the study of helminth biology is limited by the fact that some helminth parasites are too large for microinjection into the organoid lumen [11], a challenge that can be circumvented by either inverting organoid polarity [17,21] or by culturing intestinal stem cells in a two-dimensional (2D) conformation using transwells, with the apical compartment readily-available for parasite stimulation [22,23]. In fact, 2D organoid-derived epithelial monolayers (ODMs) obtained from adult stem cells of healthy duodenum faithfully replicate the cellular composition of the tissue of origin as well as its electrophysiological and permeability properties [12], providing a physiologically-relevant and experimentally-tractable platform to study the interaction between parasites that reside in the duodenum and the intestinal epithelium [22,23].

In this study, we employ human duodenal ODMs to investigate the interactions between FhNEJ and the human intestinal epithelium. This approach enables detailed functional, structural, and molecular analyses of host responses under controlled conditions, providing insights that are difficult to obtain *in*

vivo or with conventional cell lines. By applying this model, we investigate key aspects of the early host–parasite interface, including parasite attachment, epithelial barrier modulation, and intestinal epithelial responses during the initial stage of fasciolosis.

Results

FhNEJ actively engage with intestinal ODMs

First, ODMs were produced from 3D stem cell-enriched organoids derived from human duodenum using standard procedures to replicate the natural niche of FhNEJ **(Supp.** Figure 1**)**. After ODM differentiation, freshly excysted FhNEJ were obtained *in vitro* from commercially available metacercariae and added to the monolayers. Live time-lapse imaging and visual inspection revealed that FhNEJ were alive and highly motile for at least 48 h after addition to the ODMs **(Supp. Video 1)**, indicating the compatibility of the ODM system with FhNEJ viability.

Further microscopical analysis showed that the FhNEJ were in direct contact with the ODM epithelium **(**Fig. 1A**)** and employed their ventral sucker to stably attach to it **(**Fig. 1B**)**. The strength of this attachment was evidenced by the retention of FhNEJ in the preparations despite multiple washes of the ODMs during immunostaining. Strikingly, a small fraction of FhNEJ (1–3 per transwell out of 50 added) were oriented under the epithelial layer, with their ventral sucker in direct contact with the intestinal epithelial cells **(**Fig. 1C, **Supp. Video 2)**, indicating their specific recognition by the parasites.

FhNEJ compromise ODM barrier function in a dose- and time-dependent manner

The formation of a functional epithelial barrier in ODMs was shown by a constant increase in TEER overtime that stabilised 11–12 days after seeding **(**Fig. 2A**)**, consistent with previous reports [23]. At this time, ODMs were co-cultured with either 5 FhNEJ or 50 FhNEJ for 48 hours and epithelial barrier function and permeability were assessed by TEER measurements and flux assays using fluorescein. Control cultures were left untreated. At 24 hours after addition of FhNEJ, TEER had decreased in a dose-dependent manner **(**Fig. 2A**)**. Congruently, at 48 hours after infection, epithelial permeability to fluorescein was directly proportional to the number of parasites that were added to the ODMs **(**Fig. 2B**)**. We further noticed that co-incubation with 50 FhNEJ led to partial detachment of epithelial layer from the edges of the transwell filter **(**Fig. 2C, **Supp.** Figure 2**).**

To unravel whether the impairment of barrier function correlated with cell-cell barrier disruption or whether the apparent stress response of the monolayer that led to epithelial cell detachment was responsible for the decreasing TEER values, we performed immunofluorescent (IFA) and immunoblot analysis using the prototypic tight junction markers ZO-1 and CLDN-1. Results showed that treatment of ODMs with 50 FhNEJ led to a dramatic reduction in ZO-1 signal **(**Fig. 3A, **Supp.** Figure 3**)** that coincided with a significant but modest decrease in the abundance of this protein, as quantified by SDS-PAGE and immunoblotting **(**Fig. 3B,C**)**. Similarly, CLDN-1 abundance was slightly reduced upon incubation with 50

FhNEJ (Fig. 3B,C); however, the distribution of this protein to the apical domain of epithelial cells appeared unaffected (Fig. 3A, **Supp.** Figure 3).

Proteomic profiling of ODMs upon infection with FhNEJ

In parallel to the functional characterisation of epithelial barrier function in the ODMs upon stimulation with FhNEJ, we performed a proteomic analysis on whole-cell lysates of infected and control ODMs to characterise in greater detail the molecular responses that are triggered in the intestinal epithelium after 48 hours of interaction with the parasites. This analysis identified a total of 6,827 proteins with FDR ≤ 1% that were included in the differential expression analysis.

Results confirmed the dose-dependent response of ODMs to stimulation with FhNEJ, with 26 and 77 proteins differentially regulated after incubation with 5 FhNEJ (Fig. 4A, Table 1) or 50 FhNEJ (Fig. 4B, Table 2), respectively. Interestingly, 17 out of 26 of these proteins (65.4%) in ODMs treated with 5 FhNEJ were common to those identified as differentially regulated in their counterparts treated with 50 FhNEJ when compared to the untreated condition. In general, proteomic responses in the ODMs were skewed towards increased protein abundance upon incubation with the parasites, as no downregulated proteins were detected in the ODMs when incubated with 5 FhNEJ and only 4 proteins were downregulated upon incubation with 50 FhNEJ. These included the heat shock cognate 71 kDa protein (HSC70) and the S100 calcium-binding protein A10 (S100A10).

Proteins that were over-represented upon incubation with FhNEJ were involved in different biological functions. These included intercellular adhesion, as shown by increased abundance of claudin-7 (CLDN7) and nectin-1 (NECTIN1), and the immune response, reflected by enhanced levels of several innate and adaptive immune-related proteins, including the inducible T cell costimulator ligand (ICOSL, encoded by the gene ICOSLG), the protease signal peptide peptidase-like 2A (SPP2A), the receptor of the transforming growth factor β (TGFBR2), the canopy homolog 4 (CNPY4/PRAT4B), the tripartite motif-containing protein 59 (TRIM59), and copine 1 (CPN1E1). Additional information on the functions of all the identified DEPs is available in **Supp.** Table 1.

Table 1

DEPs in untreated vs. 5 FhNEJ-treated ODMs. A positive fold-change indicates that proteins were over-represented in the ODMs treated with the parasites (red). The opposite is true when the fold-change is negative (none). Proteins shaded in grey were also identified in the untreated vs. 50 FhNEJ-treated comparison (Table 2).

Gene Name	Protein Name	logFC	adjPVal
AKR7L	Aflatoxin B1 aldehyde reductase member 4	10.161	2.93E-05
GNB3	Guanine nucleotide-binding protein subunit beta-3	9.819	2.47E-06
MYO19	Unconventional myosin-XIX	9.147	5.39E-06
GAPDHS	Glyceraldehyde-3-phosphate dehydrogenase	8.876	0.000109
OR4X1	Olfactory receptor 4X1	8.768	0.000245
ARAP2	ANK repeat and PH domain-containing protein 2	8.755	3.61E-06
RGL2	Ral guanine nucleotide dissociation stimulator-like 2	8.663	0.000245
SLC44A2	Solute carrier family 44 member 2	8.539	9.51E-06
GEMIN8	Gem-associated protein 8	8.499	3.61E-06
KCNK5	Potassium channel subfamily K member 5	8.475	0.000104
MEST	Mesoderm-specific transcript homolog protein	8.360	2.14E-05
GRPEL2	GrpE protein homolog 2	8.355	0.002151
TBP	TATA-box-binding protein	8.321	2.73E-05
ADAMTSL4	ADAMTS-like protein 4	8.295	0.00017
TMEM161B	Transmembrane protein 161B	8.036	0.000216
DNAJB4	DnaJ homolog subfamily B member 4	7.982	1.07E-05
AS3MT	Arsenite methyltransferase	7.880	9.51E-06
CFLAR	CASP8 and FADD-like apoptosis regulator	7.787	1.07E-05
LDB1	LIM domain-binding protein 1	7.758	2.22E-05
TBPL1	TATA box-binding protein-like 1	7.662	0.003087
ZG16B	Zymogen granule protein 16 homolog B	7.645	0.002964
TRIM59	Tripartite motif-containing protein 59	7.531	0.00066
MED10	Mediator of RNA polymerase II transcription subunit 10	7.410	4.47E-05
CCDC61	Centrosomal protein CCDC61	7.361	9.51E-06
INO80	INO80 complex subunit A	7.314	2.73E-05

Gene Name	Protein Name	logFC	adjPVal
ENC1	Ectoderm-neural cortex protein 1	7.001	9.51E-06

Table 2

DEPs in untreated vs. 50 FhNEJ-treated ODMs. A positive fold-change indicates that proteins were over-represented in the ODMs treated with the parasites (red). The opposite is true when the fold-change is negative (blue). Proteins shaded in grey were also identified in the untreated vs. 5 FhNEJ-treated comparison (Table 1).

Gene Name	Protein Name	logFC	adjPVal
BAZ1A	Bromodomain adjacent to zinc finger domain protein 1A	12.367	8.76E-06
OR4X1	Olfactory receptor 4X1	11.056	3.46E-05
PCK1	Phosphoenolpyruvate carboxykinase	11.037	4.06E-06
ANO3	Anoctamin-3	10.341	0.001162
GAPDHS	Glyceraldehyde-3-phosphate dehydrogenase	10.112	5.85E-07
GNB3	Guanine nucleotide-binding protein subunit beta-3	9.807	5.56E-07
MYH6	Myosin-6	9.567	3.23E-06
NRAS	Transforming protein N-Ras	9.543	7.52E-07
B4GAT1	Beta-1,4-glucuronyltransferase 1	9.509	4.16E-05
ATXN7L3B	Ataxin-7-like protein 3B	9.455	0.000106
DOLPP1	Dolichyldiphosphatase 1	9.287	3.45E-06
RGL2	Ral guanine nucleotide dissociation stimulator-like 2	9.230	3.45E-06
GRPEL2	GrpE protein homolog 2	9.164	5.56E-07
TUBB8	Tubulin beta-8 chain	9.150	5.56E-07
STARD5	StAR-related lipid transfer protein 5	9.129	5.56E-07
ATP2B2	Plasma membrane calcium-transporting ATPase 4	8.941	3.35E-06
MYO19	Unconventional myosin-XIX	8.893	7.87E-07
ADAMTSL4	ADAMTS-like protein 4	8.850	2.75E-06
SENP8	Sentrin-specific protease 8	8.723	1.07E-06
ARAP2	ANK repeat and PH domain-containing protein 2	8.712	2.23E-06
SNX15	Sorting nexin-15	8.677	1.82E-06
ICOSLG	ICOS ligand	8.606	5.56E-07
NECTIN1	Nectin-1	8.554	5.4E-06
CFL2	Cofilin-2	8.530	3.88E-06
ROGDI	Protein rogdi homolog	8.518	9.78E-07

Gene Name	Protein Name	logFC	adjPVal
NOB1	RNA-binding protein NOB1	8.443	0.002346
VPS72	Vacuolar protein sorting-associated protein 72	8.364	5.56E-07
IFRD2	Interferon-related developmental regulator 2	8.332	1.98E-05
SLC44A2	Solute carrier family 44 member 2	8.327	0.000152
TMEM161B	Transmembrane protein 161B	8.313	5.56E-07
GEMIN8	Gem-associated protein 8	8.284	1.32E-05
TEAD3	TEA domain family member 3	8.257	1.48E-06
TBPL1	TATA box-binding protein-like 1	8.255	7.87E-07
CNPY4	Protein canopy homolog 4	8.231	5.56E-07
TOMM5	Mitochondrial import receptor subunit TOM5 homolog	8.199	9.89E-05
AS3MT	Arsenite methyltransferase	8.179	2.7E-06
OSCP1	Organic solute transport protein 1	8.163	5.56E-07
SPTB	Spectrin beta chain	8.162	3.35E-06
SPPL2A	Signal peptide peptidase-like 2A	8.044	0.000545
ELP6	Elongator complex protein 6	8.020	4.93E-06
EXOSC5	Exosome complex component RRP46	7.955	2.91E-05
ANKRD27	Ankyrin repeat domain-containing protein 27	7.933	0.000106
MED10	Mediator of RNA polymerase II transcription subunit 10	7.900	5.56E-07
CARNMT1	Carnosine N-methyltransferase	7.843	0.001005
LDB1	LIM domain-binding protein 1	7.827	3.27E-05
ERVK-9	Endogenous retrovirus group K member 9 Rec protein	7.775	8.97E-06
TGFBR2	TGF-beta receptor type-2	7.764	5.56E-07
CCDC61	Centrosomal protein CCDC61	7.755	7.89E-06
DNAJC30	DnaJ homolog subfamily C member 30	7.739	1.43E-05
SERPINB3	Serpin B3	7.728	0.002776
TRIM59	Tripartite motif-containing protein 59	7.668	0.000163
MEAF6	MYST/Esa1-associated factor 6	7.635	0.000106
TTL	Tubulin-tyrosine ligase	7.578	2.7E-06

Gene Name	Protein Name	logFC	adjPVal
TMEM134	Transmembrane protein 134	7.567	4.07E-06
COA4	Cytochrome c oxidase assembly factor 4 homolog	7.507	0.000102
EIF2AK3	Eukaryotic translation initiation factor 2-alpha kinase 3	7.476	5.56E-07
RRN3	RNA polymerase I-specific transcription initiation factor RRN3	7.356	1.23E-06
CPNE2	Copine-2	7.315	3.39E-06
CLDN7	Claudin-7	2.001	0.00958
VAMP3	Vesicle-associated membrane protein 3	1.534	0.024285
CDC42SE2	CDC42 small effector protein 2	1.524	0.013366
ASB15	Ankyrin repeat and SOCS box protein 15	1.344	0.010009
RPLP0	Large ribosomal subunit protein uL10	1.264	0.024651
GNPNAT1	Glucosamine 6-phosphate N-acetyltransferase	1.175	0.019083
PITPNC1	Cytoplasmic phosphatidylinositol transfer protein 1	1.128	0.001055
SH3BGRL2	SH3 domain-binding glutamic acid-rich-like protein 2	1.079	0.017617
CPNE1	Copine-1	1.072	0.005823
NEK4	Serine/threonine-protein kinase Nek4	1.014	0.047332
SFXN4	Sideroflexin-4	0.904	0.002522
ARL3	ADP-ribosylation factor-like protein 3	0.842	0.026014
POLR2E	DNA-directed RNA polymerases I, II, and III subunit RPABC1	0.795	0.038948
MED15	Mediator of RNA polymerase II transcription subunit 15	0.770	0.016588
PDK1	3-phosphoinositide-dependent protein kinase 1	0.684	0.029425
MRPS12	Small ribosomal subunit protein uS12m	-0.452	0.045035
RGS18	Regulator of G-protein signaling 18	-10.162	3.44E-06
HSPA8	Heat shock cognate 71 kDa protein	-11.677	5.56E-07
S100A10	S100 calcium-binding protein A10	-12.051	9.78E-07

Incubation of intestinal ODMs with FhNEJ-Teg does not affect epithelial barrier function

Finally, since the tegument of FhNEJ represents the outermost layer of the parasites and contains molecules that are in direct contact with host tissues [7], we stimulated ODMs with a tegument-enriched antigenic fraction of FhNEJ (FhNEJ-Teg) to determine whether the effects observed with live parasites

were mediated by surface-expressed FhNEJ effectors. To this end, increasing concentrations of FhNEJ-Teg (0–50 µg/ml) were added to differentiated ODMs and barrier integrity was assessed overtime by measuring TEER and by IFA of tight junction proteins. Results showed that none of the assayed FhNEJ-Teg concentrations induced detectable alterations in epithelial barrier function, as shown by the retention of physiological TEER (Fig. 5A) and the normal expression and distribution of the tight junction proteins ZO-1, CLDN-1, and claudin 2 (CLDN-2) (Fig. 5B). These findings indicate that surface-expressed FhNEJ molecules alone are insufficient to reproduce the effects of live parasites, highlighting that additional factors and/or physical interactions might be mediating FhNEJ-induced epithelial responses.

Discussion

Here, we examine the ability of FhNEJ to modulate intestinal barrier integrity using ODMs as a physiologically relevant system that enables the *in vitro* modelling of the intestinal stage of fasciolosis, a crucial determinant of infection success. A key advantage of this system is that it enables localised analysis of epithelial regions in close proximity to the parasites that are difficult to capture *in vivo*. Specifically, we employed epithelial monolayers derived from the human duodenum as this is the tissue that the FhNEJ encounter immediately after metacercariae excystment. Co-incubation of ODMs with live FhNEJ, but not with a tegument-enriched fraction of these parasites, revealed dose- and time-dependent impairment of barrier integrity. This effect was accompanied by modulation of tight junction components and the differential expression of proteins that might facilitate parasite migration and survival within the mammalian organism.

Tissue migration is a fundamental aspect of the biology of helminth parasites, providing significant evolutionary advantages [24]. In *F. hepatica*, this phenomenon has been primarily associated with the proteolytic and immunomodulatory activity of a vast array of secreted parasitic antigens that directly affect the integrity of host tissues [25–28]. However, no *in vitro* models currently exist that allow these mechanisms to be observed with precision. From a biomechanical perspective, during the early invasion processes of *F. hepatica*, the ventral sucker plays a significant role in parasite attachment and migration along the epithelial lining [4], but the precise mechanisms underlying trans-migration through the intestinal epithelium are currently unknown. In our study, epi- and confocal microscopy confirmed that FhNEJ actively moved over the epithelial layer employing their ventral sucker to stably attach to the ODM epithelium, consistent with the *in vivo* situation [4].

Intriguingly, observation of fixed specimens under a confocal microscope also revealed that some of the FhNEJ were recovered beneath the epithelial layer, where they reoriented their bodies so that the ventral sucker remained in contact with the epithelial cells. This behaviour suggests that FhNEJ attachment to the intestinal epithelium is not a product of random contact or passive adhesion, but rather involves active recognition and directed attachment to epithelial surfaces, potentially mediated by cues derived from host cells. As the epithelia showed detachment at the edges of the transwell filter, we believe that parasite migration beneath the epithelial cell layer most likely occurred through the transwell periphery, although we were unable to capture this phenomenon in our limited time series analysis. Given the

potent extracellular matrix (ECM)-degrading proteolytic activity of FhNEJ excreted/secreted products [29–31], it is possible that the parasites stimulate epithelial cell detachment from the underlying ECM used for transwell coating prior to cell seeding. However, further studies should confirm this hypothesis by incubating the ODMs with live FhNEJ in the presence of protease inhibitors.

Since the FhNEJ actively engaged with the ODM epithelium, we studied intestinal barrier function in this *in vitro* system. Results showed a dose- and time-dependent decrease in barrier function in ODMs incubated with the parasites as indicated by reduced TEER and increased epithelial permeability to fluorescein compared with untreated controls. Although flux assays are typically interpreted as a proxy for paracellular permeability [23,32], the observed peripheral detachment of the ODM epithelium in the presence of FhNEJ precludes any conclusion that the increased fluorescein flux reflects changes in this parameter. However, increased permeability to fluorescein upon incubation with FhNEJ coincided with a strong reduction in the apical localisation of ZO-1, a core component of tight junctions, suggesting that paracellular permeability might indeed be increased in the presence of FhNEJ [33]. Intriguingly, immunoblot analysis revealed a significant but modest decrease in ZO-1 abundance in epithelial cells incubated with 50 FhNEJ, indicating that the reduced signal observed by IFA might be a result of altered ZO-1 localisation to tight junctions rather than substantial loss of protein expression. Alternatively, co-incubation with the parasite may have also altered the structure or post-translational modifications of the protein, leading to masking of the epitope recognised by the monoclonal antibody used for immunostaining. Contrasting these results, CLDN-1 localisation to tight junctions appeared unaffected, supporting that reduced ZO-1 intensity detected in the same specimens was not due to loss of epithelial cells or technical issues during immunostaining. A similar phenotype, characterised by decreased ZO-1 but preserved CLDN-1 localisation in the colon, was reported in a mouse model of colitis [34], suggesting that this pattern may represent a broader epithelial response to stress or injury. Since incubation of the ODMs with the parasites did not apparently result in substantial cell death, loss of epithelial barrier integrity upon incubation with FhNEJ is likely caused by parasite-induced epithelium shrinkage. Interestingly, beyond its canonical role at intercellular junctions, ZO-1 regulates cytoskeletal tension, thereby modulating the forces transmitted through adhesion complexes mediating cell–ECM interactions [35]. Thus, it is possible that epithelium shrinkage is also an indirect consequence of disrupted ZO-1 localisation to tight junctions. That said, we acknowledge that our assessment of cell viability is solely based on the retention of CLDN-1 in tight junctions and cell medium acidification, which could partly be accounted for by the presence of live parasites. Further studies are needed to clarify whether FhNEJ alter paracellular permeability by interfering with tight junction integrity, and whether this could positively affect parasite migration across the intestinal epithelium.

To further elucidate broader cellular responses that are triggered in the intestinal epithelium upon FhNEJ exposure, we conducted a proteomic analysis on whole-cell lysates of ODMs incubated with 5 FhNEJ, 50 FhNEJ, or left untreated. Statistical analysis showed that proteomic reprogramming of ODMs in response to the parasites was dose-dependent, with the number of DEPs increasing in proportion to parasitic load. Due to the reduced number of DEPs identified in FhNEJ-stimulated ODMs when compared

to the uninfected controls, functional enrichment analysis did not yield any significantly-enriched gene ontology terms. However, manual examination of individual DEPs revealed several proteins of potential interest. For instance, increased abundance of intercellular adhesion molecules, including NECTIN1 and CLDN7, may reflect an epithelial attempt to strengthen the intestinal barrier in response to parasite invasion [36,37]. Although the tight junction protein ZO-1 was identified in our proteomic dataset, it was not selected by feature selection or differential expression analysis, consistent with the view that FhNEJ primarily alter the localisation of this protein to tight junctions rather than its overall abundance.

In addition, proteins related to immunity were also differentially regulated in ODMs incubated with the parasites, providing an initial clue to the immune mechanisms that operate in the intestinal epithelium in response to *F. hepatica* infection. These included increased levels of ICOSL, encoded by the gene ICOSLG, a ligand for the ICOS T cell receptor that induces T cell proliferation and cytokine secretion to stimulate the onset of T- and B-cell mediated adaptive immune responses [38]. Stimulation with FhNEJ also caused a significant increase in the abundance of SPP2A, a protease that triggers tumour necrosis factor α (TNFα)-mediated intracellular signalling cascades by cleaving this pro-inflammatory cytokine and releasing its intracellular domain [39]. Since TNFα is a central regulator of intestinal barrier integrity and inflammation [40], enhanced protein levels of SPP2A and CPN1E1, another regulator of TNFα signalling [41], may contribute to the first-line inflammatory mechanisms triggered in the intestinal epithelium in response to infection with FhNEJ.

Some immune-related proteins that were differentially regulated in ODMs upon stimulation with FhNEJ may also be associated with immune evasion mechanisms employed by these parasites. For instance, FhNEJ induced an increase in the levels of TGFBR2, a key regulator of intestinal homeostasis by promoting host tolerance to commensal microbiota [42]. This observation is consistent with the well-known ability of *F. hepatica* to stimulate TGFβ-mediated responses early after infection as a mechanism to skew host immunity towards an immunoregulatory phenotype [43]. Similarly, enhanced levels of CNPY4, a chaperone that negatively regulates toll-like receptor (TLR)-1 surface expression [44], and TRIM59, an E3 ubiquitin ligase that suppresses TLR- and type I interferon-mediated responses [45], suggests that FhNEJ may also exploit these pathways as part of their immune evasion strategy.

An interesting aspect of our proteomic analysis is that differential regulation of protein expression was substantially skewed towards increased protein abundance, regardless of the amount of FhNEJ that the ODMs were stimulated with. Strikingly, only 4 proteins were less abundant in ODMs treated with 50 FhNEJ out of the 77 total DEPs that were identified when compared to the untreated controls. One such protein was HSPA8, also known as HSC70 or HSP73, a member of the HSP70 family of chaperones. In addition to playing a central role in protein folding, HSP70 chaperones are important regulators of tight and adherens junction assembly and organisation (extensively reviewed in Ref. 46). Specifically, some HSP70 members have been described to be required for homeostatic ZO-1 expression and recruitment to tight junctions, both *in vitro* and *in vivo* [47–49]. Although, to our knowledge, no studies have directly linked HSPA8 expression to ZO-1 localisation to tight junctions, our results suggest a potential

mechanistic explanation for the ZO-1 phenotype observed in ODMs stimulated with FhNEJ, which warrants further investigation. Additionally, because ZO-1 is not only a crucial component of tight junctions but also acts as a signalling platform that influences gene expression and orchestrates mechanosensitive responses [50–53], the reduced ZO-1 localisation observed in this study may be connected to the proteomic reprogramming detected in ODMs upon stimulation with FhNEJ. Thus, modulation of tight junction dynamics may represent a mechanism by which FhNEJ regulate intestinal epithelial cell behaviour.

Another notable observation in our proteomic analysis is the strong downregulation of S100A10 in ODMs upon exposure to FhNEJ. S100A10, also known as p11, forms a heterotetrameric complex with annexin A2 at the cell surface, where it binds plasminogen (PLG) and promotes its conversion into plasmin, the key protease driving fibrinolysis [54]. Differential regulation of this central PLG receptor aligns well with our previous work showing that FhNEJ actively modulate host fibrinolysis to increase the ECM-degrading proteolytic activity surrounding the parasite, potentially facilitating trans-intestinal migration [55,56]. In this context, decreased PLG recruitment by host cells may increase its availability within the periparasitic space. Moreover, because S100A10 is required for the localisation of annexin A2 at the plasma membrane of endothelial cells [57,58], its downregulation is consistent with the reduced surface expression of annexin A2 that was previously reported in primary mouse small intestinal epithelial cells upon incubation with FhNEJ [13]. Altogether, our proteomic analysis highlights the potential of ODMs to provide mechanistic insights into how *F. hepatica* juveniles interact with the intestinal epithelium, opening exciting avenues towards a detailed characterisation of the molecular and cellular mechanisms triggered in this tissue upon infection with FhNEJ.

Finally, ODMs were incubated with increasing amounts of a tegument-enriched antigenic fraction of FhNEJ that contains molecules that are expressed within the host–parasite interface. Since the tegument of FhNEJ is in direct contact with host tissues [7], it is expected that molecules that elicit responses in intestinal cells that potentially facilitate trans-intestinal migration are mainly expressed in this antigenic compartment. To test this hypothesis, ODMs were incubated with increasing amounts of FhNEJ-Teg, which caused no detectable alterations in either the electrophysiological properties of the epithelium or the distribution of tight junction proteins, indicating that barrier function remained unaffected. These results are consistent with previous studies using the same *in vitro* system to investigate *Giardia duodenalis* pathobiology, in which barrier disruption occurred only in the presence of live parasites but not upon incubation with parasite lysates or excretory/secretory products [23,59]. Our results suggest that the physical presence of FhNEJ is required to elicit epithelial responses in the small intestine, which may represent a general mechanism among intestinal parasites that physically interact with this tissue. Supporting this idea, several proteins with established roles in mechanosensory pathways, including the TEA domain family member 3 (TEAD3) and spectrin β chain (SPTB) [60], were identified in our proteomic analysis as differentially regulated upon FhNEJ stimulation, indicating that mechanical forces exerted by the parasites are detected and transduced into signalling intracellular responses.

Although highly informative, the main limitation of the ODM co-culture system developed in this study is that host cells are seeded on polycarbonate filters that FhNEJ are unlikely to traverse; therefore, ODMs cannot yet fully replace *ex vivo* models that are currently used to study parasite trans-intestinal migration [15]. In this regard, recently developed membrane-free transwell systems where cells are seeded on hydrogels may provide a valuable *in vitro* alternative to investigate parasite migration across the intestinal barrier [61]. In the future, it will be important to assess whether similar responses are elicited in ODMs derived from additional donors and natural hosts of *F. hepatica*, such as cattle and sheep. Moreover, more sophisticated organoid-based models that better recapitulate the intestinal architecture [61,62] or variations that incorporate microbiota [63] and/or immune cells [64,65] will be key to fully capture the complexity of host–parasite interactions during early-stage fasciolosis.

In summary, this work establishes ODMs as a novel and physiologically relevant *in vitro* model that enables the functional, structural, and proteomic characterisation of the intestinal stage of *F. hepatica* infection, offering unprecedented opportunities to explore the mechanisms of tissue invasion, barrier disruption, and immune modulation by FhNEJ. This model opens a unique experimental window into the 'point of no return' of fasciolosis, when the parasite first breaches the intestinal barrier, a stage that remains poorly understood yet is central for parasite establishment and disease progression [7]. By enabling the identification of parasite effectors and host pathways involved in this critical step, ODMs may guide the discovery of early intervention targets that block the maturation of egg-laying adults, prevent disease transmission in fasciolosis hotspots, and mitigate the pathology associated with post-intestinal migration of juvenile parasites. In the long-term, these studies could ultimately inform the development of more effective and sustainable solutions to this widespread parasitic disease.

Materials and methods

In vitro excystment of *F. hepatica* metacercariae and extraction of the FhNEJ tegument-enriched protein fraction (FhNEJ-Teg)

F. hepatica metacercariae (Italian strain, Ridgeway Research Ltd) were excysted as previously described [55]. Briefly, metacercariae were incubated for 1 h at 37 ºC in a solution containing CO_2 and 0.02 M sodium dithionite (Sigma), followed by three washes with distilled water and incubation in excystment medium [Hank's balanced salt solution (Sigma) supplemented with 10% lamb bile (obtained from a local abattoir) and 30 mM HEPES (Sigma) at pH 7.4] at 37 ºC. FhNEJ were manually recovered under a stereomicroscope using a 20 µL pipette every hour after addition of excystment medium, immediately transferred to a clean plate containing ODM differentiation medium, and incubated at 37 ºC in a humidified, 5% CO_2 atmosphere to induce recovery prior to transfer to ODM cultures. The tegument-enriched antigenic fraction of FhNEJ (FhNEJ-Teg) was obtained by incubating the parasites with 1% Nonidet-P40 (Sigma) for 30 min at room temperature with mild rotation, followed by centrifugation for 5 min at 300×g, as previously described [56]. Supernatants containing the FhNEJ-Teg fraction were quantified using the Pierce BCA Protein Assay kit (Thermo Fisher) and stored at − 80 ºC until use.

Three-dimensional (3D) organoid culture

3D organoids from the human duodenum were generated previously [23] and were readily available for the present study. Three-dimensional organoid cultures **(Supp.** Figure 1A**)** were maintained by passaging once a week at a 1:3 split ratio, as previously described [23,66]. Briefly, organoids were passaged by centrifugation for 5 min at 4 ºC and 350×g, followed by chemical dissociation into single cells using TrypLE Express (Thermo Fisher Scientific) containing 10 µM Y-27632 (ROCK inhibitor; Tocris) for 5 min at 37 ºC. Single cells were centrifuged for 5 min at 4 ºC and 500×g and resuspended in an appropriate volume of organoid growth medium [23] mixed with Cultrex basement membrane extract (Bio-Techne) at a 1:2 ratio. Next, 50 µl of cell suspension was seeded into each well of a 24-well plate and incubated at 37°C for 30 min to allow polymerisation of the basement membrane extract. Cells were cultured in 500 µl of organoid growth medium at 37 ºC in a humidified, 5% CO_2 atmosphere and medium was replaced every two days. Organoid medium was prepared as previously described [23], with minor modifications in composition [59]. Specifically, organoid medium consisted of 50% Wnt3a/R-Spondin-3/Noggin (WRN) conditioned medium (ATCC, CRL-3276), 20% RSpondin-1 conditioned medium (kindly provided by Calvin Kuo, Stanford University), 10% mNoggin conditioned medium (kindly provided by Hans Clevers, Utrecht University), 50 ng/ml human recombinant EGF (Peprotech), 10 mM HEPES (Thermo Fisher Scientific), 2 mM stable glutamine (Capricorn), 100 µg/ml streptomycin, 100 U/ml penicillin (Capricorn), 1x NCS21 (Capricorn), 250 ng/ml biotin (Roth), 1x N2 (Capricorn), 1 mM N-acetylcysteine (Sigma), 10 mM nicotinamide (Sigma), 500 nM A83-01 (Sigma), and 10 µM SB202190 (Cayman Chemicals) in Advanced DMEM/F-12 (Thermo Fisher Scientific). Y-27632 (Tocris) was added to cell culture medium to inhibit anoikis and removed the day after seeding.

Generation of two-dimensional (2D) organoid-derived epithelial monolayers (ODMs)

Organoid-derived epithelial monolayers (ODMs) were generated from 3D duodenum organoids following established protocols [23,66] **(Supp.** Figure 1B**)**. Specifically, 7-day old organoid cultures were dissociated as previously described and 5×10^5 cells were seeded in cell culture transwell inserts (0.6 cm^2, 0.4 µm pore size; MilliCell) pre-coated with a mixture of Cultrex basement membrane extract (Bio-Techne) and DMEM/F-12 (Thermo Fisher Scientific) at a 1:20 ratio. Both sides of the transwell system were supplied with ODM differentiation medium (organoid growth medium lacking WRN-conditioned medium, A83-01, and SB202190), which was exchanged every two days, and ODMs were incubated at 37 ºC in a humidified, 5% CO_2 atmosphere.

Establishment of the co-culture system

Eleven to twelve days after ODM seeding, either 5 or 50 live FhNEJ obtained from freshly-excysted metacercariae or different concentrations of FhNEJ-Teg (0–50 µg/ml) were added to the apical compartment of the transwell inserts and incubated at 37 ºC in a humidified, 5% CO_2 atmosphere. Care was taken to ensure that the final volume of cell medium in the apical compartment after stimulation was identical across all experimental conditions. ODMs left untreated served as negative controls, and

ODMs treated apically with 2 µM of the apoptosis inducer staurosporine (Tocris) were used as positive controls for epithelial barrier breakdown, as previously described [23]. Each independent experiment was performed using three transwell filters per condition, with two filters used for immunofluorescence analysis and one filter for the preparation of ODM whole-cell lysates. Forty-eight hours after stimulation, cell culture supernatants were carefully aspirated, and whole-cell lysates were prepared by adding 200 µl of 2×Laemmli buffer [4% (w/v) sodium dodecyl sulfate (SDS), 20% (v/v) glycerol, 0.004% (w/v) bromophenol blue, 0.125 M Tris-HCl (pH 6.8), 50 mM dithiothreitol (DTT)] containing cOmplete protease inhibitor cocktail (Roche) to the cells, followed by shaking at room temperature for 20 min and boiling at 95 ºC for 10 min. Samples were stored at − 20 ºC until use. The viability of FhNEJ was confirmed throughout the entire stimulation period in all the experiments by monitoring their active motility under a stereoscope.

Measurement of transepithelial electric resistance (TEER)

Transepithelial electric resistance (TEER) was measured 3 hours after ODM seeding and every 24 hours thereafter using a Millicell ERS-2 Voltohmmeter (Merck-Millipore) equipped with an Ag/AgCl electrode (STX01; Merck-Millipore) on a heating block set to 37 ºC. Resistance values from blank (cell-free) transwell inserts were subtracted from raw readings and adjusted to a surface area of 1 cm^2, as previously described [23,59], and either expressed as absolute values or relative to the time of stimulation with FhNEJ (t_0).

Fluorescein flux assay

Forty-eight hours after stimulation, and prior to fixation or lysis, 100 µM of fluorescein (332 Da, Sigma) diluted in 400 µl of ODM differentiation medium was added apically and samples of 20 µl from the basal compartment were taken in triplicate at 0 min (before fluorescein addition), 10 min, 20 min, 30 min, and 40 min after addition of fluorescein. Next, 80 µl of milliQ water were added to each medium sample and fluorescence intensity (485 nm/525 nm) was measured in an Infinite M200 PRO plate reader (Tecan Life Sciences). Intensities were calculated relative to the basal values recorded prior to fluorescein addition (0 min, t_0).

Immunofluorescent analysis and confocal microscopy

Cell culture supernatants from the ODMs were carefully aspirated and the cells were immediately fixed with either 4% paraformaldehyde (PFA) for 1 hour at 37 ºC or ice-cold 20% methanol for 40 min at − 20 ºC. PFA-fixed cells were permeabilised for 20 min at room temperature in 1×Tris-buffered saline (TBS) containing 0.25% (v/v) of Triton X-100 and 0.1 M glycine and both PFA- and methanol-fixed samples were blocked for 1 hour at room temperature with blocking buffer [1×TBS, 0.05% (v/v) Tween-20, 0.02% (v/v) Triton X-100, 3% (w/v) bovine serum albumin, 1% (v/v) normal goat serum, and 0.02% NaN_3]. Primary antibodies (anti-ZO-1, BD Biosciences, cat. nr. 610967, 1:250, methanol fixation; anti-CLDN-1, Life Technologies cat. nr. 727800, 1:100, methanol fixation) were diluted in blocking buffer and added to the

transwell inserts overnight at 4 ºC. After three washes in wash buffer (1×TBS containing 0.05% Tween-20 and 0.02% Triton X-100), the corresponding fluorophore-conjugated secondary antibodies produced in goat were diluted in blocking buffer containing 10 µM 4',6-diamidino-2-phenylindole (DAPI) and added to the samples for 1 hour at room temperature. Phalloidin-iFluor 647 reagent (Abcam) was added to the corresponding PFA-fixed wells for 1 hour at room temperature to label F-actin filaments. The samples were then washed three times in wash buffer, mounted into glass slides in Fluoromount-G mounting medium (Invitrogen) and imaged in a Leica Stellaris 8 confocal laser scanning microscope (Leica Microsystems) equipped with 405 nm diode laser and Leica white light laser. Imaging was performed with HC PL APO 40×/1.10 W motCORR CS2 and HC PL APO 63×/1.40 OIL CS2 objectives using the LAS X software, version 4.4.0.24861 (Leica Microsystems). Five stacks spanning the full epithelial depth were acquired per transwell insert with a step size of 1 µm and frame averaging of 2. Images were processed using the FIJI software, version 2.15.0 [67], and the contrast was equally adjusted across experimental conditions for visualisation purposes. To improve visual intensity discrimination across experimental conditions, images were displayed using the Fire lookup table, which color-codes signal intensity in a single fluorescence channel. In this scheme, higher-intensity pixels are represented in white/yellow and lower-intensity pixels in blue, facilitating contrast detection on a black background.

SDS-polyacrylamide gel electrophoresis (SDS-PAGE) and immunoblotting

Equal volumes of samples were loaded into 4–20% Bis-Tris pre-cast gels (GenScript) and separated in MOPS buffer (GenScript) at constant 200 V. Proteins were then transferred onto nitrocellulose membranes (GE Healthcare) in Tris-Glycine transfer buffer containing 2% methanol and 0.01% SDS (v/v) using standard procedures. Transfer quality was validated by Ponceau S total protein staining. Membranes were then blocked for 1 hour at room temperature in 5% skimmed milk (w/v) diluted in phosphate-buffer saline (PBS) and membranes were incubated overnight at 4 ºC with primary antibodies diluted in PBS containing 0.05% Tween-20 (Sigma; PBS-T) and 5% skimmed milk (w/v; BioRad). Membranes were then washed three times with PBS-T and incubated for 1 hour at room temperature with the respective HRP-conjugated secondary antibodies diluted in PBS-T containing 5% skimmed milk (w/v; BioRad). After three washes in PBS-T, protein bands were detected by enhanced chemiluminescence using the SuperSignal West Dura Extended Duration Substrate (Thermo Fisher) according to the manufacturer's instructions. The following primary antibodies and dilutions were used: anti-ZO-1, Invitrogen cat. nr. 61-7300, 1:200; anti-CLDN-1, Life Technologies cat. nr. 71-7800, 1:500; anti-Ezrin, Abcam cat. nr. ab4069, 1:500; and anti-GAPDH, Poreintech cat. nr. 600004-1-Ig, 1:500. Band intensities were quantified using the FIJI software, version 2.15.0 [67]. To improve quantification accuracy, SDS-PAGE and immunoblotting were performed in technical duplicate, and ZO-1 and CLDN-1 band intensities were normalised to both Ezrin (Abcam) and GAPDH (Proteintech) and then averaged.

Live imaging of ODMs stimulated with FhNEJ

Organoid-derived cells were seeded into tissue culture inserts (0.6 cm^2, 0.4 µm pore size; CellQART) pre-coated with Cultrex basement membrane extract (Bio-Techne) and stimulated with 25 FhNEJ obtained

from freshly-excysted metacercariae, as described above. Live-cell imaging was performed on a Zeiss Axio Observer.Z1 inverted microscope (Carl Zeiss) equipped with an ApoTome structured illumination system. Environmental conditions were maintained at 37 ºC and 5% CO_2 using an Incubator XL multi S2 (Pecon) TempModule S with Heating Unit XL S and CO_2 Module S (Carl Zeiss). Images were acquired using a Zeiss EC Plan-Neofluar 10×/0.30 objective, a Colibri 7 LED light source, and a HE DsRed filter cube (Carl Zeiss), with an AxioCam 820 mono camera (Carl Zeiss). Time-lapse imaging with tiles 4×4 was performed, acquiring one image every 5 min for approximately 16 hours. Image acquisition and processing were carried out with ZEN software, version 3.8.1 (Carl Zeiss).

Proteomic analysis of ODM whole-cell lysates

Sample preparation. Protein concentrations were determined using the Macherey-Nagel Protein Quantification Assay (Macherey-Nagel) and equal amounts of protein were reduced with 2 mM dithiothreitol at 60 ºC for 20 min, and alkylated with 5 mM iodoacetamide diluted in 50 mM ammonium bicarbonate at room temperature for 30 min. Next, proteins were purified using the SP3 protocol [68,69] to eliminate detergents prior to in solution protein digestion. Purified proteins were digested overnight at 37 ºC with 100 ng of sequencing-grade trypsin (Promega) diluted in 50 mM ammonium bicarbonate and the reaction was stopped by addition of 0.1% trifluoroacetic acid.

LC-MS/MS analysis. Liquid chromatography (LC) was performed by loading 200 ng of digested peptides (diluted in 20 µL of 0.1% formic acid) onto an Evotip Pure tip (EvoSep) following the manufacturer's instructions, followed by separation using the Evosep One system on an analytical column Performance 15 cm×150 µm, 1.5 µm (Evosep). The eluted peptides were ionised in a captive Spray with 1700 V at 200 ºC and tandem mass spectrometry analysis (MS/MS) was performed in a TimsTOF fleX mass spectrometer (Bruker) in data-independent acquisition Parallel Accumulation-Serial Fragmentation (diaPASEF) mode.

Data processing and protein quantification. The PASER system (Bruker) was used to send the raw data for subsequent analysis and quantification with DIA-NN v1.8 software (https://github.com/vdemichev/DiaNN). First, an *in silico*-predicted spectral library was built from the SwissProt_Human database using DIA-NN v1.8 and using QuantUMS (high precision) as the quantification strategy. After raw data normalisation and quantification, proteins were filtered at ≤ 1% false discovery rate (FDR) to ensure confidence in protein identification. The proteomic analysis was carried out at the Proteomics Unit of the Central Support Service for Experimental Research (SCSIE) of the University of Valencia (Spain), a member of the Instituto de Salud Carlos III (ISCIII) ProteoRed Proteomics Platform.

Statistical analysis. Comparison of protein expression levels between FhNEJ-treated and control ODMs included feature pre-selection through dimensionality reduction and penalised regression, allowing the reliable identification of condition-specific gene and protein expression patterns in high-dimensional datasets [70–73]. In parallel, differential expression analysis to get fold-change and *p*-values for individual

proteins was performed with a series of statistical principles that outperform ordinary *t*-tests in proteomics data analysis when sample size is limiting [74,75].

Specifically, peak intensities of all the conditions were transformed to the logarithm with base *e* using the log1p function in R. Next, a stringent statistical pipeline employing three distinct methodologies was applied to identify differentially expressed proteins (DEPs) with high robustness, as previously described [55,76]. First, the glmnet package in R was employed to fit an elastic-net regularised regression model to select those variables (proteins) that better explained each experimental condition [77] **(Supp.** Figure 4A,B**)**. To refine the model, the nearZeroVar function from the caret package in R was applied to identify variables with near-zero variance, indicating very low variability across observations. These proteins were discarded from subsequent analysis. The values of the regularisation parameters (alpha and lambda) were optimised with the train function of the caret package through cross-validation re-sampling to obtain the regularised model that best fitted our data. The log-transformed expression values of the selected proteins were standardised through Z-score normalisation to ensure direct comparability of protein expression levels across samples, followed by representation in heatmaps. Second, feature selection by elastic-net was validated through Partial Least Squares Discriminant Analysis (PLS-DA) using the mixOmics package in R [78] **(Supp.** Figure 4C**)**. This package contains the 'variable importance in the projection' (vip) function, which estimates the importance of each variable in the projection. When vip > 1.5, the influence of the variable on the response is very high [55,76]. Third, differential expression analysis between selected pairs of experimental conditions was performed using the limma package in R to get fold-change (FC) differences in protein expression along with the corresponding *p*-values [74]. Only proteins that were selected by both elastic-net and PLS-DA (vip > 1.5) and exhibited a significant fold-change (p-value ≤ 0.05), as calculated by limma, were considered differentially regulated. Graphical representation of this analysis was performed using volcano plots generated in R software with the *ggplot2* and *ggrepel* packages. This analysis was performed by the Statistics and Omics Data Analysis Unit of the Central Support Service for Experimental Research (SCSIE) of the University of Valencia, Spain.

Statistical analyses

Plots were created, and statistical analyses were performed using Prism 10 software, version 10.5.0 (GraphPad Software). Data points and graph bars represent the mean of three biological or technical replicates. Error bars represent either the standard error of the mean (SEM) or the standard deviation (SD) to reflect the precision of the sample mean as an estimate of the population mean or the variability among individual technical measurements, respectively. Comparisons between more than two experimental groups were performed via one-way or two-way analysis of variance (ANOVA) followed by Tukey post-hoc analysis for pairwise comparisons. Unless otherwise stated, the differences were not significant.

Declarations

Acknowledgements

JGM and MSL acknowledge funding received from projects ULYSSES (RTI2018-093463-J-100) and PERSEUS (PID2023-152150OB-C21) funded by MICIU/AEI/10.13039/501100011033 and FEDER, EU, and URANUS (CNS2022-135561) funded by MICIU/AEI/10.13039/501100011033 and NextGenerationEU/PRTR. We thank Silvio Bürge (ZBS4 Advanced Light and Electron Microscopy, Robert Koch Institute) for setting up and optimising the live imaging of FhNEJ on the ODMs, Gudrun Kliem for technical assistance, Prof. Dr. Susanne Krug (University Hospital Charité, Berlin) for her excellent support on organoid technologies, and Raquel Gavidia (SCSIE, Valencia, Spain) for the statistical analysis of proteomics data. JS thanks the regional government of the Junta de Castilla y León for her predoctoral contract and the European Molecular Biology Organization (EMBO) for financial support through a Scientific Exchange Grant (SEG number 10280) to perform the experiments presented in this study. We also acknowledge support from Project CLU-2025-2-02—IRNASA_CSIC Unit of Excellence, funded by the Regional Government of Castilla y León and co-financed by the European Regional Development Fund (ERDF, Europe drives our growth), as well as Project DEEP-MaX-2024_IRNASA, funded by the Spanish National Research Council (CSIC).

References

1. Mas-Coma, S., Valero, M.A., Bargues, M.D.: Fascioliasis. In: Toledo, R., Fried, B. vol (eds.) Digenetic Trematodes, vol. 1154, pp. 71–103. Springer International Publishing (2019)
2. Fitzpatrick, J.L.: Global food security: the impact of veterinary parasites and parasitologists. Vet. Parasitol. **195**, 233–248 (2013)
3. Nyindo, M., Lukambagire, A.-H.: Fascioliasis: an ongoing zoonotic trematode infection. *BioMed Res. Int.* 786195 (2015). (2015)
4. Sangster, N.C., Martínez-Moreno, Á., Pérez, J.: Chapter 5. Pathology, pathophysiology and clinical aspect. in *Fasciolosis* 145–180CABI, UK, (2022). 10.1079/9781789246162.0000
5. Andrews, S.J., Cwiklinski, K., Dalton, J.P.: Chapter 1. The discovery of *Fasciola hepatica* and its life cycle. in *Fasciolosis* 1–23CABI, UK, (2022). 10.1079/9781789246162.0000
6. World Health Organization: Ending the neglect to attain the Sustainable Development Goals: A road map for Neglected Tropical Diseases 2021–2030. (2020). https://www.who.int/publications/i/item/9789240023680
7. González-Miguel, J., Becerro-Recio, D., Siles-Lucas, M.: Insights into *Fasciola hepatica* juveniles: crossing the fasciolosis rubicon. Trends Parasitol. **37**, 35–47 (2021)
8. Siles-Lucas, M., Becerro-Recio, D., Serrat, J., González-Miguel, J.: Fascioliasis and fasciolopsiasis: Current knowledge and future trends. Res. Vet. Sci. **134**, 27–35 (2021)
9. Kelley, J.M., et al.: Current threat of triclabendazole resistance in *Fasciola hepatica*. Trends Parasitol. **32**, 458–469 (2016)

10. Toet, H., Piedrafita, D.M., Spithill, T.W.: Liver fluke vaccines in ruminants: strategies, progress and future opportunities. Int. J. Parasitol. **44**, 915–927 (2014)
11. Duque-Correa, M.A., Maizels, R.M., Grencis, R.K., Berriman, M.: Organoids - new models for host-helminth interactions. Trends Parasitol. **36**, 170–181 (2020)
12. Weiß, F., et al.: Human duodenal organoid-derived monolayers serve as a suitable barrier model for duodenal tissue. Ann. N Y Acad. Sci. **1515**, 155–167 (2022)
13. Becerro-Recio, D., et al.: Proteomics coupled with *in vitro* model to study the early crosstalk occurring between newly excysted juveniles of *Fasciola hepatica* and host intestinal cells. PLoS Negl. Trop. Dis. **16**, e0010811 (2022)
14. López-García, M., et al.: Deciphering the proteomic profile of the parasite *Fasciola hepatica* after initial vertebrate host infection reveals new insights into its early-stages. Mol. Cell. Proteom. MCP. **101005** (2025). 10.1016/j.mcpro.2025.101005
15. Becerro-Recio, D., et al.: Study of the migration of *Fasciola hepatica* juveniles across the intestinal barrier of the host by quantitative proteomics in an *ex vivo* model. PLoS Negl. Trop. Dis. **16**, e0010766 (2022)
16. European Commission: Directive 2010/63/EU of the European Parliament and of the Council of 22 September 2010 on the Protection of Animals Used for Scientific Purposes. (2010). https://eur-lex.europa.eu/legal-content/EN/TXT/?uri=celex%3A32010L0063
17. Smith, D., et al.: T e development of ovine gastric and intestinal organoids for studying ruminant host-pathogen interactions. Front. Cell. Infect. Microbiol. **11**, 733811 (2021)
18. Duque-Correa, M.A., et al.: Development of caecaloids to study host–pathogen interactions: new insights into immunoregulatory functions of *Trichuris muris* extracellular vesicles in the caecum. Int. J. Parasitol. **50**, 707–718 (2020)
19. Faber, M.N., et al.: Development of bovine gastric organoids as a novel *in vitro* model to study host-parasite interactions in gastrointestinal nematode infections. Front. Cell. Infect. Microbiol. **12**, 904606 (2022)
20. Vitkauskaite, A., et al.: *In vitro* co-culture of *Fasciola hepatica* newly excysted juveniles (NEJs) with 3D HepG2 spheroids permits novel investigation of host-parasite interactions. Virulence. **16**, 2482159 (2025)
21. Chapuis, A.F., et al.: Characterization of bovine and ovine basal-out and apical-out ileum organoids. R Soc. Open. Sci. **12**, 250326 (2025)
22. Duque-Correa, M.A., et al.: Defining the early stages of intestinal colonisation by whipworms. Nat. Commun. **13**, 1725 (2022)
23. Holthaus, D., et al.: Dissection of barrier dysfunction in organoid-derived human intestinal epithelia induced by *Giardia duodenalis*. Gastroenterology. **162**, 844–858 (2022)
24. Read, A.F., Skorping, A.: The evolution of tissue migration by parasitic nematode larvae. Parasitology. **111**(Pt 3), 359–371 (1995)

25. Robinson, M.W., Menon, R., Donnelly, S.M., Dalton, J.P., Ranganathan, S.: An integrated transcriptomics and proteomics analysis of the secretome of the helminth pathogen *Fasciola hepatica*. Mol. Cell. Proteom. **8**, 1891–1907 (2009)
26. Cwiklinski, K., et al.: The cathepsin-like cysteine peptidases of trematodes of the genus *Fasciola*. In: Advances in Parasitology, vol. 104, pp. 113–164. Elsevier (2019)
27. De Verissimo, M.: *Fasciola hepatica* serine protease inhibitor family (serpins): Purposely crafted for regulating host proteases. PLoS Negl. Trop. Dis. **14**, e0008510 (2020)
28. Dalton, J.P., Robinson, M.W., Mulcahy, G., O'Neill, S.M., Donnelly, S.: Immunomodulatory molecules of *Fasciola hepatica*: candidates for both vaccine and immunotherapeutic development. Vet. Parasitol. **195**, 272–285 (2013)
29. Cwiklinski, K., et al.: Infection by the helminth parasite *Fasciola hepatica* requires rapid regulation of metabolic, virulence, and invasive factors to adjust to its mammalian host. Mol. Cell. Proteom. **17**, 792–809 (2018)
30. Di Maggio, L.S., et al.: Across intra-mammalian stages of the liver fluke *Fasciola hepatica*: a proteomic study. Sci. Rep. **6**, 32796 (2016)
31. Robinson, M.W., et al.: Collagenolytic activities of the major secreted cathepsin L peptidases involved in the virulence of the helminth pathogen, *Fasciola hepatica*. PLoS Negl. Trop. Dis. **5**, e1012 (2011)
32. Fiorentino, M., et al.: *Helicobacter pylori*-induced disruption of monolayer permeability and proinflammatory cytokine secretion in polarized human gastric epithelial cells. Infect. Immun. **81**, 876–883 (2013)
33. Van Itallie, C.M., Fanning, A.S., Bridges, A., Anderson, J.M.: ZO-1 stabilizes the tight junction solute barrier through coupling to the perijunctional cytoskeleton. Mol. Biol. Cell. **20**, 3930–3940 (2009)
34. Poritz, L.S., et al.: Loss of the tight junction protein ZO-1 in dextran sulfate sodium induced colitis. J. Surg. Res. **140**, 12–19 (2007)
35. Haas, A.J., et al.: ZO-1 Guides tight junction assembly and epithelial morphogenesis via cytoskeletal tension-dependent and -independent functions. Cells **11**, (2022)
36. Fukuhara, A., et al.: Role of nectin in organization of tight junctions in epithelial cells. Genes Cells Devoted Mol. Cell. Mech. **7**, 1059–1072 (2002)
37. Ding, L., et al.: Inflammation and disruption of the mucosal architecture in claudin-7-deficient mice. Gastroenterology. **142**, 305–315 (2012)
38. Roussel, L., Vinh, D.C.: ICOSL in host defense at epithelial barriers: lessons from ICOSLG deficiency. Curr. Opin. Immunol. **72**, 21–26 (2021)
39. Friedmann, E., et al.: SPPL2a and SPPL2b promote intramembrane proteolysis of TNFalpha in activated dendritic cells to trigger IL-12 production. Nat. Cell. Biol. **8**, 843–848 (2006)
40. Ruder, B., Atreya, R., Becker, C.: Tumour Necrosis Factor alpha in intestinal homeostasis and gut related diseases. Int. J. Mol. Sci. **20**, (2019)

41. Tomsig, J.L., Sohma, H., Creutz, C.E.: Calcium-dependent regulation of tumour necrosis factor-alpha receptor signalling by copine. Biochem. J. **378**, 1089–1094 (2004)
42. Ihara, S., Hirata, Y., Koike, K.: TGF-β in inflammatory bowel disease: a key regulator of immune cells, epithelium, and the intestinal microbiota. J. Gastroenterol. **52**, 777–787 (2017)
43. Donnelly, S., Flynn, R., Mulcahy, G., O'Neill, S.: Chapter 9. Immunological interaction between *Fasciola* and its host. in *Fasciolosis* 278–308CABI, UK, (2022). 10.1079/9781789246162.0000
44. Hart, B.E., Tapping, R.I.: Cell surface trafficking of TLR1 is differentially regulated by the chaperones PRAT4A and PRAT4B. J. Biol. Chem. **287**, 16550–16562 (2012)
45. Kondo, T., Watanabe, M., Hatakeyama, S.: TRIM59 interacts with ECSIT and negatively regulates NF-κB and IRF-3/7-mediated signal pathways. Biochem. Biophys. Res. Commun. **422**, 501–507 (2012)
46. Lechuga, S., et al.: Regulation of epithelial and endothelial barriers by molecular chaperones. Cells **13**, (2024)
47. Yuan, X., et al.: The heat shock protein 70 plays a protective role in sepsis by maintenance of the endothelial permeability. *BioMed Res. Int.* 2194090 (2020). (2020)
48. Kong, Q., et al.: HSPA12B Attenuated acute myocardial ischemia/reperfusion injury via maintaining endothelial integrity in a PI3K/Akt/mTOR-dependent mechanism. Sci. Rep. **6**, 33636 (2016)
49. Wang, Y., et al.: Distinct roles of intracellular heat shock protein 70 in maintaining gastrointestinal homeostasis. Am. J. Physiol. Gastrointest. Liver Physiol. **314**, G164–G178 (2018)
50. González-Mariscal, L., et al.: Tight junctions and the regulation of gene expression. Dev. Urogenit. Syst. MTOR Signal. Tight Junctions Health Dis. **36**, 213–223 (2014)
51. McCrea, P.D., Gu, D., Balda, M.S.: Junctional music that the nucleus hears: cell-cell contact signaling and the modulation of gene activity. Cold Spring Harb Perspect. Biol. **1**, a002923 (2009)
52. Zihni, C., Mills, C., Matter, K., Balda, M.S.: Tight junctions: from simple barriers to multifunctional molecular gates. Nat. Rev. Mol. Cell. Biol. **17**, 564–580 (2016)
53. Haas, A.J., Karakus, M., Zihni, C., Balda, M.S., Matter, K.: ZO-1 regulates hippo-independent YAP activity and cell proliferation via a GEF-H1- and TBK1-regulated signalling network. Cells **13**, (2024)
54. Hedhli, N., et al.: The annexin A2/S100A10 system in health and disease: emerging paradigms. *J. Biomed. Biotechnol.* 406273 (2012). (2012)
55. Serrat, J., et al.: Early host–parasite interaction models reveal a key role for fibrinolysis in *Fasciola hepatica* intestinal migration. Parasit. Vectors. **18**, 387 (2025)
56. Serrat, J., et al.: *Fasciola hepatica* juveniles interact with the host fibrinolytic system as a potential early-stage invasion mechanism. PLoS Negl. Trop. Dis. **17**, e0010936 (2023)
57. Deora, A.B., Kreitzer, G., Jacovina, A.T., Hajjar, K.A.: An annexin 2 phosphorylation switch mediates p11-dependent translocation of annexin 2 to the cell surface. J. Biol. Chem. **279**, 43411–43418 (2004)
58. Powell, M.A., Glenney, J.R.: Regulation of calpactin I phospholipid binding by calpactin I light-chain binding and phosphorylation by p60v-src. Biochem. J. **247**, 321–328 (1987)

59. Hagen, K.D., et al.: *Giardia*'s domed ventral disc architecture is essential for attachment and contributes to epithelial barrier disruption. Mol. Biol. Cell. **36**, ar93 (2025)
60. Harvey, K.F., Tang, T.T.: Targeting the Hippo pathway in cancer. Nat. Rev. Drug Discov. **24**(11), 852–869 (2025)
61. Hofer, M., Duque-Correa, M.A., Lutolf, M.P.: Patterned gastrointestinal monolayers with bilateral access as observable models of parasite gut infection. Nat. Biomed. Eng. **9**, 1075–1085 (2025)
62. Nikolaev, M., et al.: Homeostatic mini-intestines through scaffold-guided organoid morphogenesis. Nature. **585**, 574–578 (2020)
63. Puschhof, J., et al.: Intestinal organoid cocultures with microbes. Nat. Protoc. **16**, 4633–4649 (2021)
64. Recaldin, T., et al.: Human organoids with an autologous tissue-resident immune compartment. Nature. **633**, 165–173 (2024)
65. Lawrence, A.-L.E., et al.: Neutrophil prime unique transcriptional responses in intestinal organoids during infection with nontyphoidal Salmonella enterica serovars. *mSphere* 9, e0069324 (2024)
66. Warschkau, D., et al.: From 3D to 2D: Harmonization of protocols for two-dimensional cultures on cell culture inserts of intestinal organoids from various species. Bio-Protoc. **12**, e4295 (2022)
67. Schindelin, J., et al.: Fiji: an open-source platform for biological-image analysis. Nat. Methods. **9**, 676–682 (2012)
68. Moggridge, S., Sorensen, P.H., Morin, G.B., Hughes, C.S.: Extending the compatibility of the SP3 paramagnetic bead processing approach for proteomics. J. Proteome Res. **17**, 1730–1740 (2018)
69. Hughes, C.S., et al.: Single-pot, solid-phase-enhanced sample preparation for proteomics experiments. Nat. Protoc. **14**, 68–85 (2019)
70. Ebrahimi, V., et al.: Predictive determinants of overall survival among re-infected COVID-19 patients using the elastic-net regularized Cox proportional hazards model: a machine-learning algorithm. BMC Public. Health. **22**, 10 (2022)
71. Janizek, J.D., et al.: Uncovering expression signatures of synergistic drug responses via ensembles of explainable machine-learning models. Nat. Biomed. Eng. **7**, 811–829 (2023)
72. Torang, A., Gupta, P., Klinke, D.J.: 2nd. An elastic-net logistic regression approach to generate classifiers and gene signatures for types of immune cells and T helper cell subsets. BMC Bioinform. **20**, 433 (2019)
73. Zhang, K., et al.: Machine learning–based prediction of survival prognosis in esophageal squamous cell carcinoma. Sci. Rep. **13**, 13532 (2023)
74. Ritchie, M.E., et al.: limma powers differential expression analyses for RNA-sequencing and microarray studies. Nucleic Acids Res. **43**, e47 (2015)
75. Kammers, K., Cole, R.N., Tiengwe, C., Ruczinski, I.: Detecting Significant Changes in Protein Abundance. EuPA Open. Proteom. **7**, 11–19 (2015)
76. Pinheiro, T., et al.: Differential proteomic analysis by SWATH-MS unravels the most dominant mechanisms underlying yeast adaptation to non-optimal temperatures under anaerobic conditions.

Sci. Rep. **10**, 22329 (2020)

77. Friedman, J., Hastie, T., Tibshirani, R.: Regularization paths for generalized linear models via coordinate descent. J. Stat. Softw. **33**, 1–22 (2010)
78. Rohart, F., Gautier, B., Singh, A., Lê Cao, K.-A., mixOmics: An R package for 'omics feature selection and multiple data integration. PLoS Comput. Biol. **13**, e1005752 (2017)

Unsectioned Paragraphs

*Correspondence: javier.gonzalez@irnasa.csic.es

Figures

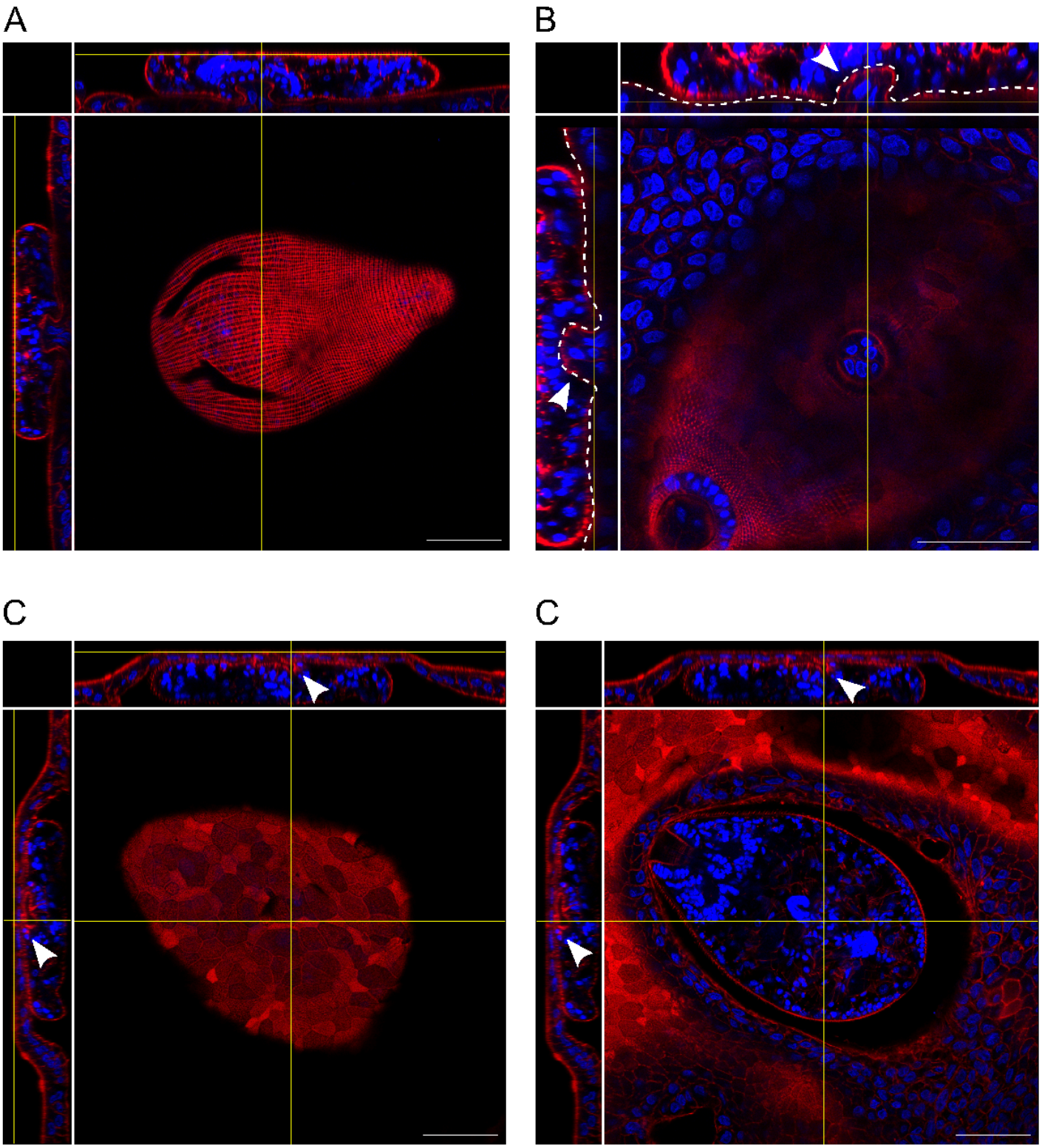

Figure 1

Incubation of ODMs with live FhNEJ. Forty-eight hours after addition of FhNEJ, ODMs were fixed, stained for IFA and visualised by confocal microscopy. Phalloidin (red) was used to highlight the actin filaments present in the apical border of epithelial cells and the surface and internal muscle fibres of FhNEJ. DAPI (blue) was used to visualise nuclear DNA. Specimens were visualised in a Leica Stellaris 8 confocal microscope using the 40× objective. **A,B)** The FhNEJ were mostly found on the apical side of the

epithelium, in direct contact with epithelial cells and attached to them via their ventral sucker (arrowheads). In B, the interface between the parasite and the epithelial layer has been underlined with a white dashed line. **C)**Occasionally, some FhNEJ were recovered under the epithelial layer (*left panel*, apical plane of the projection; *right panel*, middle plane of the projection). In panels B and C, arrowheads indicate the FhNEJ ventral sucker. Scale bars, 50 µm.

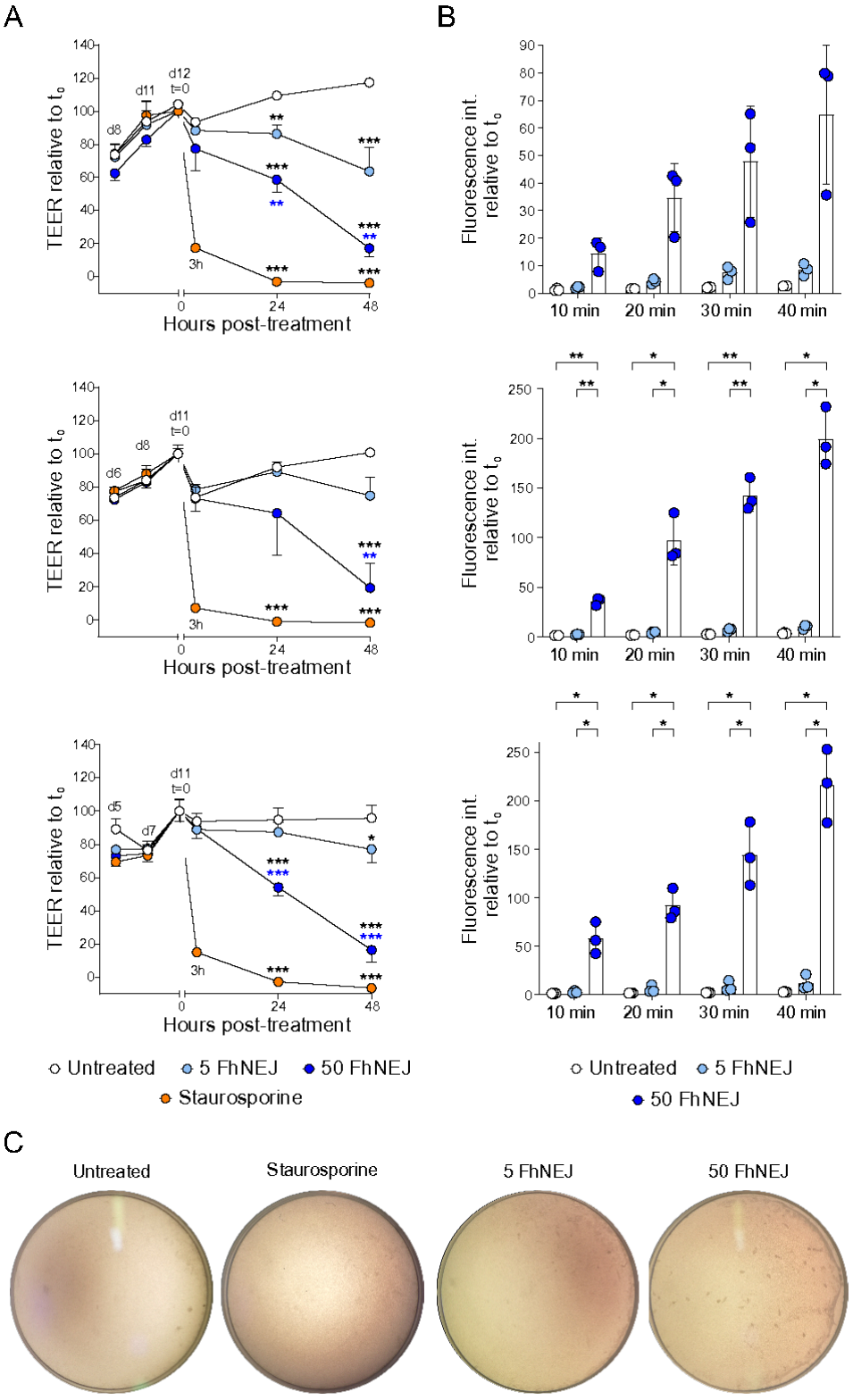

Figure 2

Incubation of ODMs with FhNEJ results in a dose- and time-dependent decrease in epithelial barrier function. A) Dose- and time-dependent decrease in TEER after stimulation with FhNEJ. Treatment of ODMs with the apoptosis-inducer staurosporine (2 µM) served as a positive control for epithelial barrier breakdown. The results of three independent experiments are shown. Three successive passages of duodenal 3D organoids and freshly excysted *F. hepatica* metacercariae were used in each independent experiment. Data points indicate the mean of three technical replicates ± SD. Black asterisks indicate significant differences between the indicated groups and the untreated condition, and blue asterisks indicate significant differences between ODMs treated with 5 FhNEJ and 50 FhNEJ (**p<0.01; ***p<0.001; one-way ANOVA). **B)** Fluorescein flux into the basal compartment of ODMs was measured 48 hours after infection at 10, 20, 30, and 40 minutes following fluorescein addition to the apical compartment. Results for staurosporine-treated samples are not shown as they displayed maximal fluorescence intensity (between 100× and 300× higher than t_0) at the earliest timepoint. The results of three independent experiments are shown. Three successive passages of duodenal 3D organoids and freshly excysted *F. hepatica* metacercariae were used in each independent experiment. Bars indicate the mean of three technical replicates ± SD, and asterisks indicate significant differences between the indicated groups (*p<0.05; **p<0.01; two-way ANOVA). **C)** Representative stereoscope images of ODMs incubated with 5 FhNEJ, 50 FhNEJ, or left untreated 48 hours after addition of the parasites.

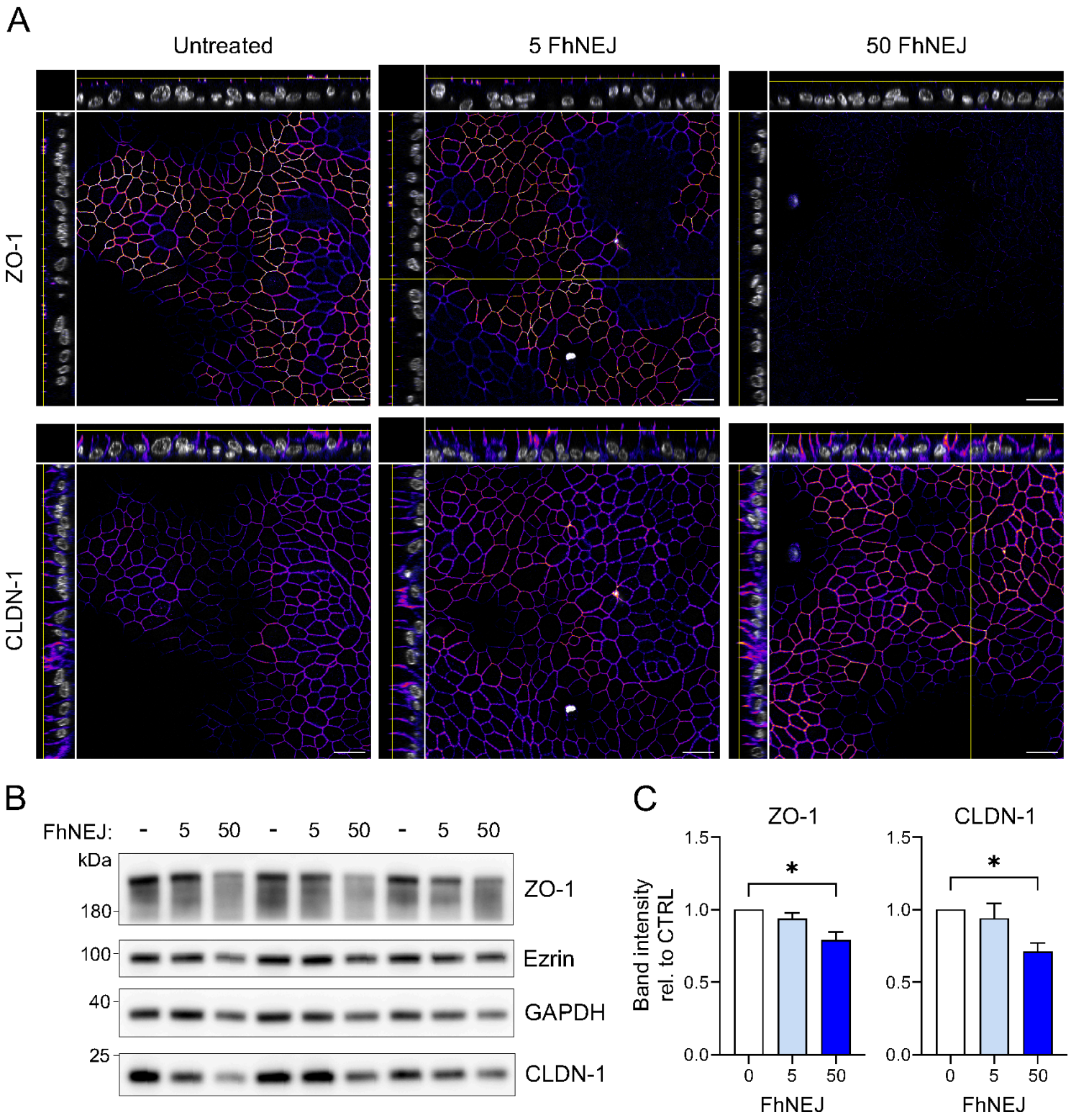

Figure 3

Incubation of ODMs with high doses of FhNEJ affects ZO-1 localisation at the apical domain of intestinal epithelial cells. A) Orthogonal stacks of representative IFA images of tight junction proteins ZO-1 and CLDN-1 48 hours after addition of FhNEJ. ZO-1 and CLDN-1 are displayed with colour-coded intensities. DAPI is shown in greyscale. Specimens were visualised in a Leica Stellaris 8 confocal microscope using the 63× objective. Scale bars, 20 µm. **B)** Immunoblot analysis of tight junction proteins ZO-1 and CLDN-1

48 after addition of FhNEJ. Results are shown for three independent experiments. Ezrin and glyceraldehyde phosphate dehydrogenase (GAPDH) served as loading controls. **C)** Quantification of band intensity normalised to Ezrin and GAPDH, across two technical replicates and three independent experiments. Bars indicate the mean ± SEM of three independent experiments ($p<0.05$; one-way ANOVA).

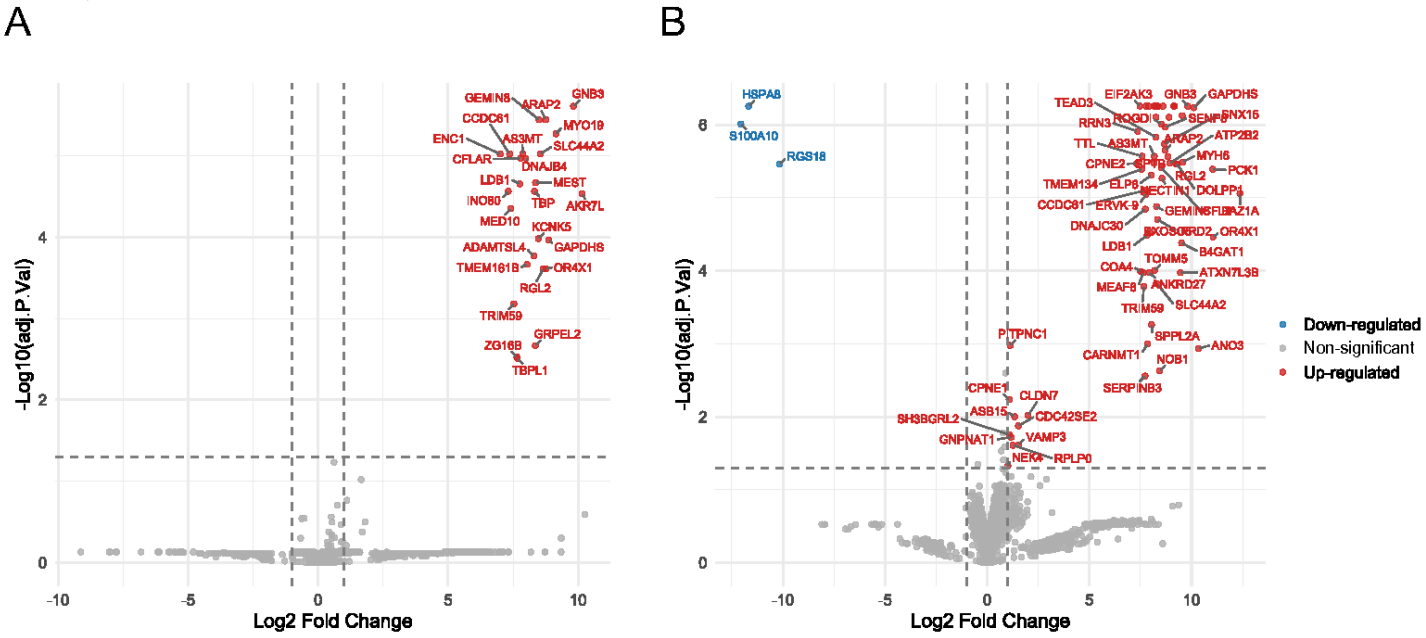

Figure 4

Differentially abundant proteins in ODMs following FhNEJ stimulation. Volcano plots showing the proteins that were detected as differentially abundant in ODMs incubated with 5 FhNEJ **(A)** or 50 FhNEJ **(B)** when compared to untreated controls. The p-value cut-off is set at ≤0.05. For visualization purposes, identities are shown only for proteins with |FC| ≥ 1.

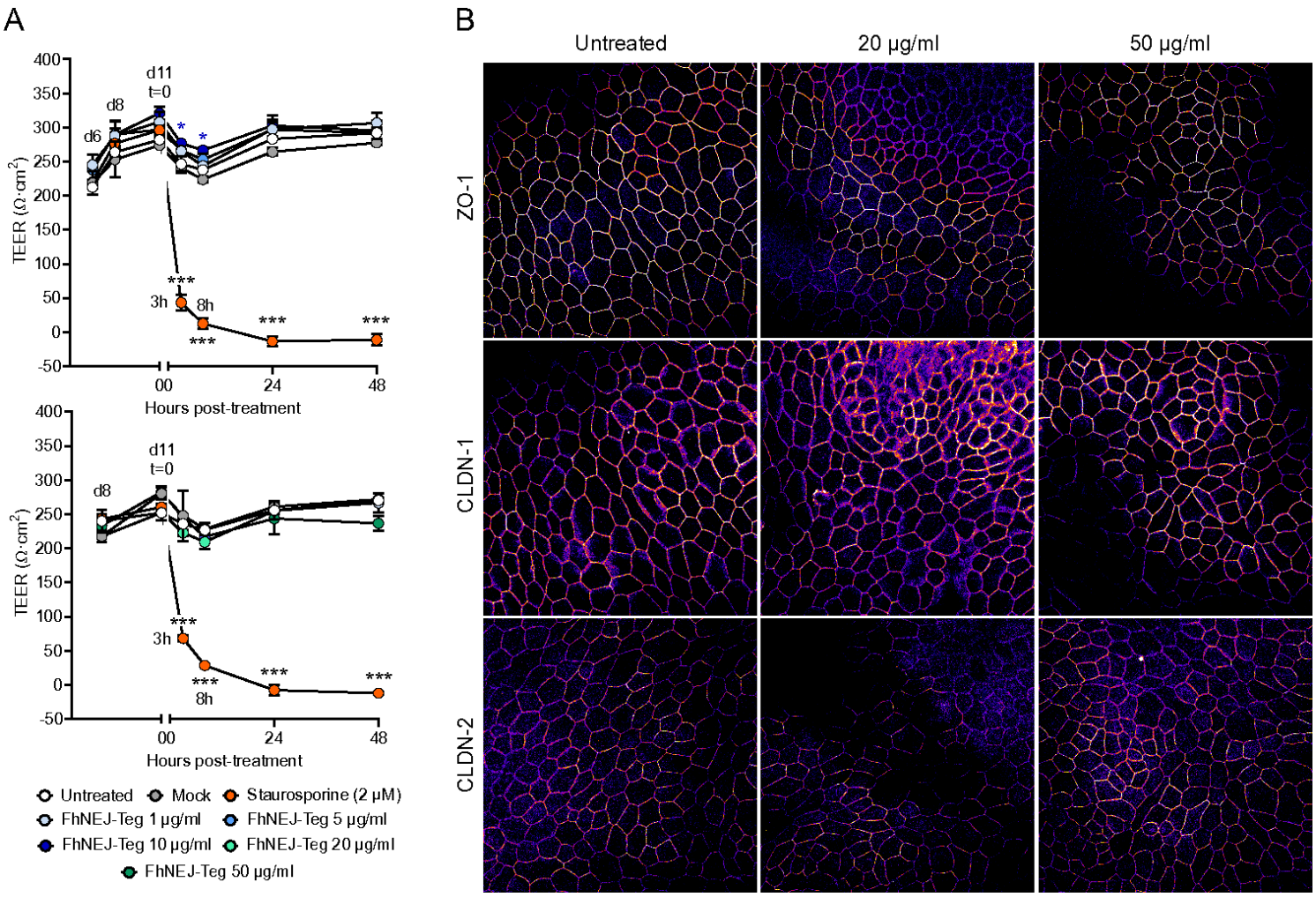

Figure 5

Incubation of ODMs with FhNEJ-Teg does not affect barrier function. A) Time- and dose-dependent evolution of TEER in ODMs treated with increasing amounts of FhNEJ-Teg. Data points indicate the mean of three technical replicates ± SD, and asterisks indicate significant differences between the indicated groups and the untreated condition (*p<0.05; ***p<0.001; one-way ANOVA). **B)** Representative IFA images of the tight junction proteins ZO-1, CLDN-1, and CLDN-2 at 72 hours after ODM stimulation with 20 µg/ml and 50 µg/ml of FhNEJ-Teg. Images show a single channel displayed with colour-coded intensities. DAPI is shown in greyscale. Specimens were visualised in a Leica Stellaris 8 confocal microscope using the 63× objective. Scale bars, 20 µm.

Supplementary Files

This is a list of supplementary files associated with this preprint. Click to download.

- Supplementaryinformationlinks.pdf